FULL PAPER

Hybrid-organic-inorganic anatase as a bifunctional catalyst for enhanced production of HMF from glucose in water

Carlos A. S. Lanziano[a,b], Silvia F. Moya[a], Dean. H. Barrett[a], Erico Teixeira-Neto[c], Reginaldo Guirardello[b], Felipe Souto da Silva,[e] Roberto Rinaldi,*[d] Cristiane B. Rodella*[a]

Abstract: Herein, we report a synthetic route for the preparation of hybrid-organic-inorganic anatase (hybrid-TiO_2) via a facile hydrothermal synthesis method employing citric acid. The synthetic approach results in a high surface area nanocrystalline anatase polymorph of TiO_2. The uncalcined hybrid-TiO_2 is directly studied here as the catalyst for the conversion of glucose into HMF. In the presence of the hybrid-TiO_2, HMF yields up to 45% at glucose conversions up to 75% were achieved in water at 130 ^oC in a monophasic batch reactor. As identified by Ti K-edge XANES, hybrid-TiO_2 contains a large fraction of five-fold coordinatively unsaturated Ti(IV) sites, which act as the Lewis acid catalyst for the conversion of glucose into fructose. As citric acid is anchored in the structure of hybrid-TiO_2, carboxylate groups seem to catalyse the sequential conversion of fructose into HMF. The fate of citric acid bounded to anatase and the Ti(IV) Lewis acid sites throughout recycling experiments is also investigated. In a broader context, the contribution outlines the importance of hydrothermal synthesis for the creation of water-resistant Lewis acid sites for the conversion of sugars. Most importantly, the utilisation of the hybrid-TiO_2 with no calcination step contributes to dramatically decreasing the energy consumption in the catalyst preparation.

Introduction

5-Hydroxymethylfurfural (HMF) plays an important role in the development of the emerging bio-based economy. Owing to its structural features, HMF can be used as a platform chemical in the production of biofuels, pharmaceuticals and polymers.[1–4] In aqueous media, HMF can be obtained from either fructose or glucose in the presence of heterogeneous catalysts.[1,4–9] Nonetheless, HMF selectivity is low (~12%) due to the formation of levulinic acid, formic acid as well as humins.[1,6,8] Glucose is both widely available and cheaper than fructose. Thus, glucose is often the preferred starting material for the production of HMF.[3] In this context, bifunctional catalysts capable of isomerising glucose into fructose and sequentially converting fructose into HMF are required [1,4,10–15]

To improve the conversion of glucose into HMF, several strategies—such as microwave-assisted heating,[7] hot compressed water,[9] biphasic reaction systems,[16,17] and ionic liquids as the reaction media[18]—have been investigated. Regarding the utilisation of multifunctional catalysts,[5,6,9,15,19–24] anatase (TiO_2) holds promise as a catalyst for the high-yield production of HMF from glucose owing to several unique features.[5,7,8,23,25] For instance, anatase shows a higher surface area, compared to the rutile and brookite polymorphs. Furthermore, the active sites required for the conversion of fructose into HMF are also present on TiO_2 anatase phase.[5–7,15,23,25–27] In fact, Hara and co-workers showed that TiO_2 contains water-tolerant Lewis acid sites, owing to the presence of coordinatively unsaturated Ti(IV) on the oxide surface.[6,26,28–30]

Motivated by the findings concerning the water-tolerant Lewis acidity of anatase, we designed an anatase synthesis in the presence of citric acid (CA) in excess, i.e. CA:Ti(IV)=1.1 mol/mol. Under this condition, we hypothesised that the formation of Lewis sites should be maximised because of the stabilising effect of CA on the particle formation, which prevents the growth of the anatase crystallites and should also generate defects in the structure. In addition, as the hybrid-TiO_2 is not calcined, but employed in the reaction as synthesised, it is plausible to expect that the hybrid-organic-inorganic anatase (hybrid-TiO_2) will feature the presence of Brønsted acid sites derived from the presence of CA's free carboxylic groups.

Herein, we demonstrate hybrid-TiO_2 to be a highly efficient catalyst for the direct production of HMF from glucose in water. This report is organised into five parts. The first compares the structural and textural properties of hybrid-TiO_2 against those from regular anatase obtained from the hydrolysis of titanium(IV) isopropoxide. Ti K-edge XANES results reveal hybrid-TiO_2 to contain a fraction of five-fold coordinatively unsaturated Ti(IV) sites larger than that of regular anatase. The second presents the catalytic results. Hybrid-TiO_2 allows for HMF yields up to nine-times higher than those achieved by regular anatase in water. The third part presents the co-operation of CA and anatase in the catalytic system, indicating that the coordinatively unsaturated Ti(IV) is associated with the isomerisation of glucose to fructose, while citric acid anchored on the anatase structure is responsible for the conversion of fructose into HMF. The fourth part shows the results of recycling experiments, demonstrating the good stability of the hybrid-TiO_2 catalyst. Finally, in the fifth part, in-depth characterisation of hybrid-TiO_2 by using Ti K-edge XANES and TGA-MS reveal the fate of the Lewis and Brønsted acid sites throughout the catalyst recycling.

[a] Mr. C. A. S. Lanziano, Dr. S. F. Moya, Dr. D. H. Barrett and Dr. C. B. Rodella*
Brazilian Synchrotron Light Laboratory (LNLS)
Brazilian Centre for Research in Energy and Materials (CNPEM)
CP 6192, CEP 13083-970, Campinas, SP, Brazil
Email: cristiane.rodella@lnls.br
[b] Mr. C. A. S. Lanziano, Dr. R. Guirardello
School of Chemical Engineering
University of Campinas
Av. Albert Einstein, 500, CEP 13083-852, Campinas, SP, Brazil
[c] Dr. E. T.-Neto
Brazilian Nanotechnology National Laboratory (LNNano)
Brazilian Centre for Research in Energy and Materials (CNPEM)
CP 6192, CEP 13083-970, Campinas, SP, Brazil
[d] F. de Souta da Silva, Dr. R. Rinaldi
Department of Chemical Engineering, Imperial College London
South Kensington Campus, SW7 2AZ, United Kingdom
Email: rrinaldi@ic.ac.uk

Supporting information available on www

Results and Discussion

To explore our working hypothesis regarding the effect of CA on the structural and textural features of hybrid-TiO_2, the material properties of hybrid-TiO_2 were compared against those of anatase obtained from a conventional hydrolysis route beginning with titanium(IV) isopropoxide with no added CA. This material (regular 'inorganic' anatase) is referred to as "i-TiO_2."

Material characterisation

Both hybrid-TiO_2 and i-TiO_2 show diffraction patterns characteristic of anatase phase (Figure 1). However, the XRD pattern for the hybrid-TiO_2 exhibits broadened reflections peaks, indicating that this material is formed by crystallites smaller than those from i-TiO_2. In fact, the average crystallite sizes are 5 nm and 10 nm for hybrid-TiO_2 and i-TiO_2, respectively as presented in Table 1.

Table 1. Textural properties and average crystallite size of i-TiO_2 and hybrid-TiO_2

Material	BET specific area (m^2g^{-1})	Pore volume (cm^3g^{-1})	BHJ average pore diameter (nm)	Mean crystalline size[a] (nm)
i-TiO_2	105	0.14	8.4	10
Hybrid-TiO_2	376	0.30	3.2	5

[a] Estimated from XRD data.

Displayed in Figure 2 are the HR-TEM images of the TiO_2 catalysts. In good agreement with the crystallite sizes estimated from XRD data, HR-TEM images show i-TiO_2 consists of independent crystallites of 8-15 nm in size, while hybrid-TiO_2 is an agglomerate of very small crystallites (2-5 nm). The small crystallite size of hybrid-TiO_2 is associated with the strong interaction of citric acid and Ti(IV) species. There is abundant evidence that carboxylic acid ligands, which are released during the condensation of titanium complexes, adsorb readily onto the freshly-forming surface of TiO_2 hindering the particle growth.[31–33] This process is expected to create O^{2-} vacancies on Ti(IV) centre, i.e. Lewis acid sites.

The textural properties of the materials were investigated by N_2 adsorption-desorption isotherm profiles (Figure 3). Table 1 summarises the textural properties. Hybrid-TiO_2 exhibits type IV isotherm, indicating the presence of ink-bottle-shaped mesopores. By contrast, i-TiO_2 shows a mixed type II and type IV isotherm, indicating the presence of non-structural meso/macroporosity in addition to structural ink-bottle-shaped mesopores. Markedly, hybrid-TiO_2 exhibits a surface area 3.6-times larger than that of i-TiO_2. Furthermore, the pore volume of hybrid-TiO_2 is twice as large as that of i-TiO_2. Both materials exhibit a wide pore-size distribution as shown in Figure S1, Supporting Information.

To assess the nature of acid sites created by the synthetic methodologies, infrared (IR) absorption spectra from pyridine adsorbed on hybrid-TiO_2 and i-TiO_2 were collected (Figure 4). Prior to the adsorption of pyridine, these materials were evacuated at 120°C for 22 h under dynamic vacuum ($2{\cdot}10^{-5}$ mbar). CA in hybrid-TiO_2 is stable under these conditions, as revealed by TGA-MS analysis (*vide infra*, Figure 8).

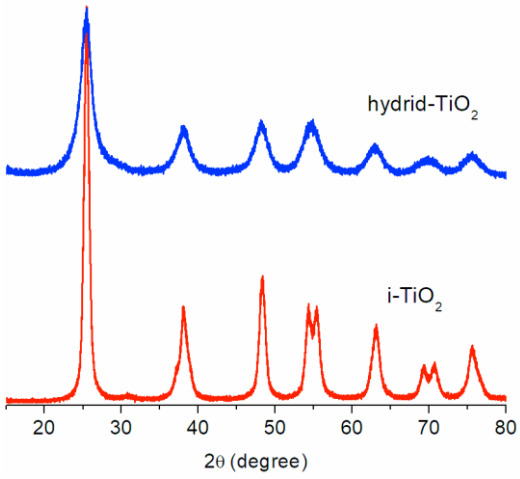

Figure 1. XRD patterns of hybrid-TiO_2 and i-TiO_2 exhibiting anatase phase.

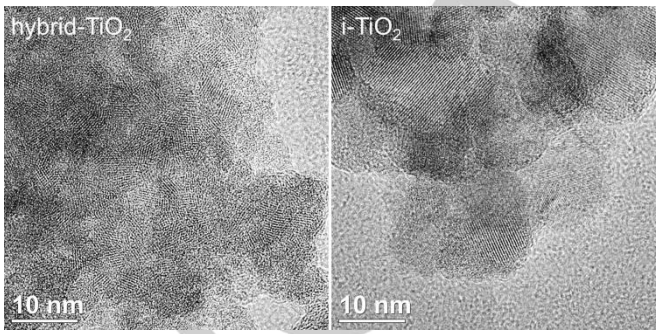

Figure 2. HR-TEM images of hybrid-TiO_2 and i-TiO_2 xerogels.

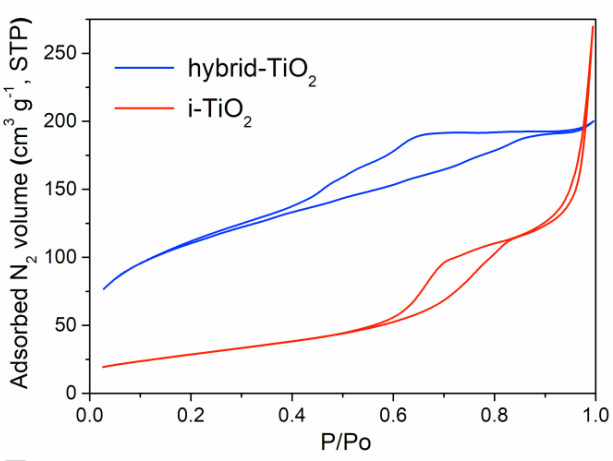

Figure 3. N_2 adsorption-desorption isotherms of the i-TiO_2 and hybrid-TiO_2.

Unfortunately, both CA and citrate ions show IR adsorption bands in the same region of the characteristic bands for adsorbed pyridine (IR spectrum of hybrid-TiO_2 displayed in grey colour in Figure 4; detailed signal assignment listed in Table S1). Despite this, it was possible to identify the presence of both Brønsted (1540 and 1640 cm^{-1}, regions highlighted in blue colour)[45] and

Lewis (1444 and 1602 cm^{-1}, regions highlighted in green colour)[45] acid sites on hybrid-TiO_2 surface. Clearly, the band intensities for both Brønsted and Lewis acid sites are stronger for hybrid-TiO_2 than those found for i-TiO_2. This observation suggests that a larger quantity of both acid sites is present in hybrid-TiO_2, which may be attributable to the larger surface area of hybrid-TiO_2.

Considering the Brønsted acid sites, hybrid-TiO_2 exhibits a much more intense band for pyridinium ion, compared against i-TiO_2. More importantly, it is apparent that there is a ligand exchange occurring on Ti(IV) centre upon exposing hybrid-TiO_2 to pyridine ('Py'). In fact, the spectrum of pyridine adsorbed on hybrid-TiO_2 also displays a very intense IR absorption band characteristic for R-COOH species (centred at about 1675 cm^{-1}: region highlighted in pale red colour), while the spectrum of evacuated hybrid-TiO_2 only shows the characteristic IR bands for the carboxylate ion form (broad band between 1320 and 1450 cm^{-1} and shoulder at 1530 cm^{-1}). We rationalise these observations in the IR spectra to correspond to a release of carboxylate ligands from Ti(IV) centre, enabling the chemical equilibrium $R\text{-}COO^- + (Ti\text{-}OH_2)^+ \leftrightharpoons R\text{-}COOH + (Ti\text{-}OH)$ to be established on the surface. Overall, these observations suggest important features of the interaction between CA/citrate and Ti(IV) in hybrid-TiO_2. Thermodynamically, the fact that pyridinium ion ('PyH^+') exhibits a pK_a value of 5.25 close to those of CA pK_a values (pK_{a1} 3.13, pK_{a2} 4.76 and pK_{a3} 6.40) implies that appreciable quantities of both R−COOH and $[RCOO^-][pyH^+]$ species are present on the surface, as pinpointed by IR spectroscopy. Kinetically, the fact that the characteristic IR band of R−COOH is present in the spectrum of pyridine adsorbed on hybrid-TiO_2 strongly suggests that the interaction between Ti(IV) and some populations of $RCOO^-$ groups is labile, enabling the co-existence of Lewis [Ti(IV)—□, where '□' denotes a vacancy] and Brønsted acid sites (R—COOH or Ti—OH_2^+) in equilibrium on the surface under the reaction conditions.

To provide further insight into the local order of Ti(IV) in i-TiO_2 and hybrid-TiO_2, Ti-edge XANES analyses were performed. Normalised Ti-edge XANES results are presented in Figure 5. The pre-edge features present are highly sensitive to subtle changes in the Ti(IV) chemical environment. These features are closely related to the degree of *d*–*p* orbital mixing, and the distortion of the centrosymmetric environment on Ti.[34,35] The pre-edge peaks denoted by 'P_1', 'P_2', 'P_2'' and 'P_3' correspond to the dipole-forbidden transitions 1*s* to 3*d*–4*p* hybrid orbitals, characteristic of Ti(IV) ions with a pseudo-octahedral symmetry as that of anatase. Most importantly, according to Farges et al.,[36] P_2 and P_2' peaks are related to the presence of five-fold coordinated Ti(IV) centres (TiO_5). When exposed to the surface, these centres can act as Lewis acid sites. Compared to i-TiO_2, hybrid-TiO_2 has a larger quantity of such five-fold coordinated Ti(IV) centres, as indicated by the stronger intensity of the P_2' peak in the hybrid-TiO_2 XANES spectrum. This finding agrees well with the more intense IR pyridine absorption bands characteristic for Lewis acid sites. Furthermore, pyridine adsorbed on Lewis acid sites of hybrid-TiO_2 presents a blueshift by 5 cm^{-1} relative to that on i-TiO_2 (hybrid-TiO_2: 1607 cm^{-1} *vs.* i-TiO_2: 1602 cm^{-1}; Figure 4). This finding indicates that Py···Ti(IV) interaction is slightly stronger in hybrid-TiO_2 than i-TiO_2, in line with Ti K-edge XANES, which demonstrates hybrid-TiO_2 to present more coordinatively unsaturated Ti(IV) sites than i-TiO_2.

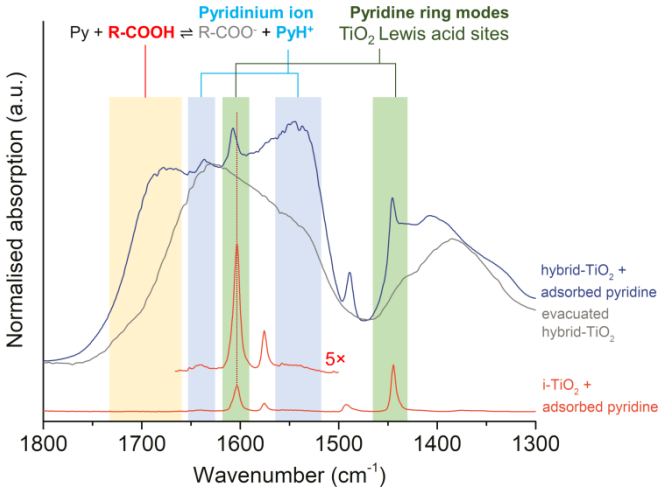

Figure 4. Infrared absorption spectra from pyridine adsorbed on hybrid-TiO_2 and i-TiO_2. The FTIR spectrum displayed in greyish colour corresponds to that of the evacuated hybrid-TiO_2 (in this case, the band at 1626 cm^{-1} corresponds to remnant water chemisorbed on TiO_2, detailed band assignment listed in Table S1). The red-dotted line at 1602 cm^{-1} serves as an eye guide to better show the blueshift observed for hybrid-TiO_2 in the band characteristic of the interaction of pyridine and TiO_2 Lewis acid sites.

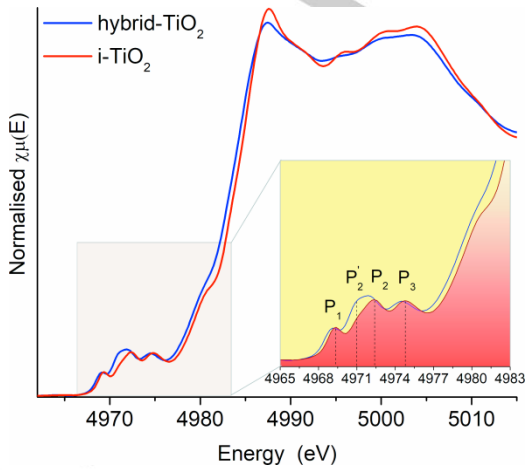

Figure 5. Normalised Ti K-edge XANES spectra of i-TiO_2 and hybrid-TiO_2.

Catalyst results

Catalytic performance of hybrid-TiO_2 and i-TiO_2 was evaluated for the conversion of glucose into HMF in water. Figure 6 compares the catalysts with respect to the temporal evolution of glucose conversion and fructose and HMF formation at temperatures of 120, 130 and 140 °C. In general, hybrid-TiO_2 showed an HMF productivity higher than i-TiO_2 under all conditions studied here. At 120 °C for 7 h, glucose conversions of 34% and 48%, respectively, for i-TiO_2 and hybrid-TiO_2 were achieved (Figure 6a and 6d). However, HMF yield was only 5% for i-TiO_2, while 19% for TiO_2-HYD (Figure 6a and 6d). Total selectivity to minor identified selectivity to minor identified products (levulinic acid, formic acid, and furfural) was lower than 1%. Increasing the reaction temperature to 130 °C, HMF production increased with both catalysts. Notably, however, is the superior performance of hybrid-TiO_2. In fact, while with i-TiO_2 catalyst HMF yields varied from (Figure 6b and 6e) 3 to 8% after 0.5 to 7 h respectively, with

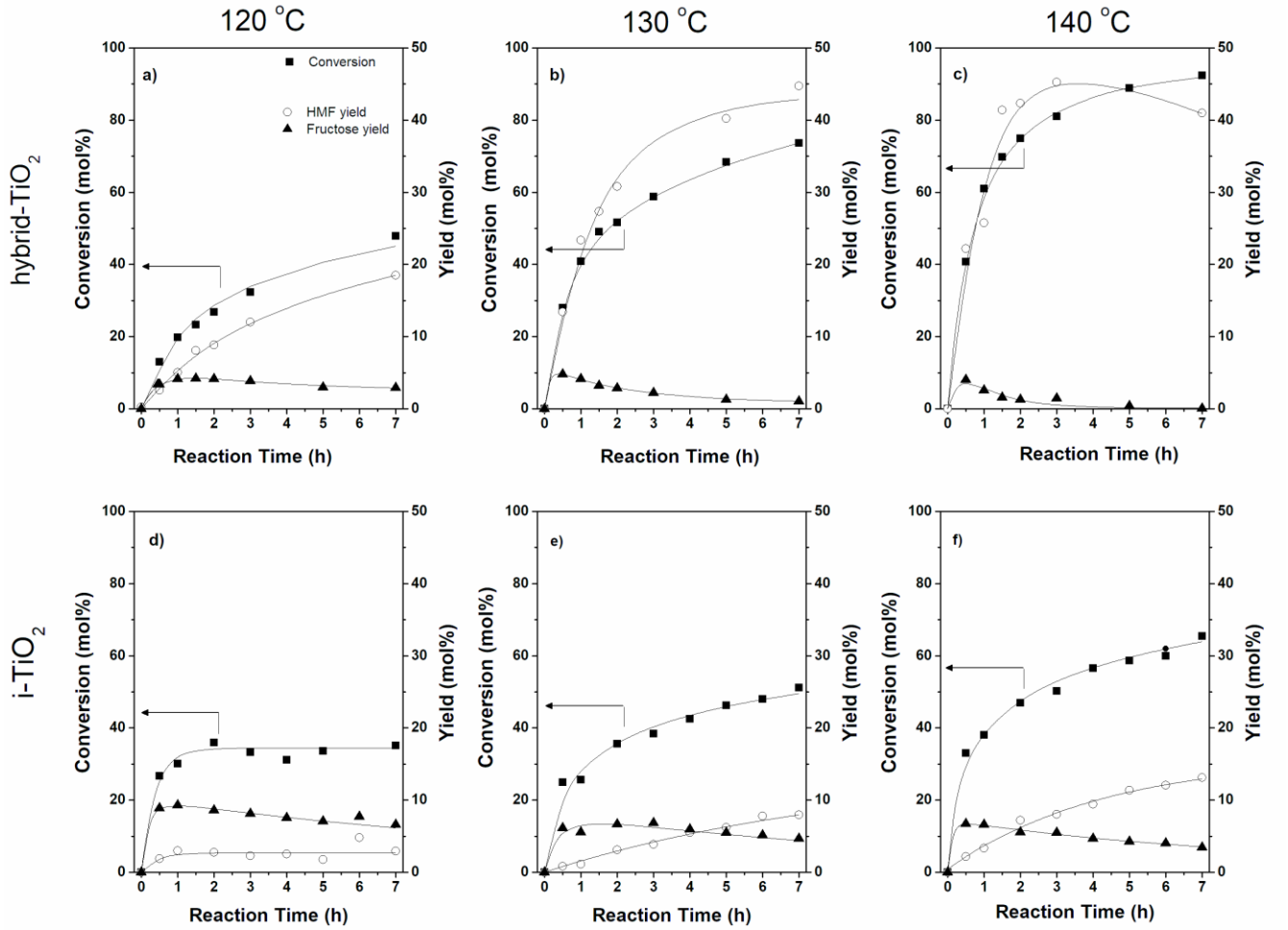

Figure 6. Catalytic activity for the conversion of glucose and yields of HMF and fructose at 120 (A and D), 130 (B and E) and 140 °C (C and F) for hybrid-TiO_2 (top) and i-TiO_2 (bottom). Reaction conditions: water (160 mL), glucose (3.26 g), catalyst (i-TiO_2 or hybrid-TiO_2, 2.7 g), 500 rpm.

hybrid-TiO_2 HMF yields from 14 to 45% were achieved under the same conditions. Conversion attained at 130 °C for i-TiO_2 and hybrid-TiO_2 was 48 and 77%, respectively (Figure 6b and 6e). Finally, at 140 °C the conversion of glucose was 64% and 92% for i-TiO_2 and hybrid-TiO_2, respectively (Figure 6c and 6f). Nonetheless, a corresponding improvement in the HMF yield was not observed. Indeed, at 140 °C, a 45% HMF yield in the presence of hybrid-TiO_2 catalyst was achieved, which implies 56% selectivity at an 81% conversion after 3 h. At high conversions, HMF yield decreases owing to HMF conversion to levulinic acid (releasing formic acid), which accounts for approx. 3% glucose equivalent consumption. The formation of humins constitutes, however, the main route of HMF degradation in our system at high glucose conversions, in line with previous observations from various catalytic systems. [1,4,6,8]

Kitano et al.[37] reported 14% HMF yield for glucose conversion performed in the presence of titanate nanotubes with large surface area [i.e. 400 $m^2\ g^{-1}$; reaction conditions: catalyst (0.05 g), glucose (0.05 g), water (10 mL), temperature (120 °C), 3 h]. The authors attributed the superior catalytic activity of the titanate nanotubes, compared to the other titania-based catalysts, to the large numbers of Lewis acid sites and the presence of effective Brønsted sites as well as the porous structure of the catalyst.

Recently, a notable result was also reported by Dutta et al. [7], using mesoporous TiO_2 nanospheres obtained via a sodium salicylate templating method, which allowed for the preparation of high surface area materials (324 $m^{-2}\ g^{-1}$). In that study, a 25% HMF yield was obtained using a microwave-assisted heating (120 °C for 5 min). Improved yields were attained (up to 37%) when dimethyl sulfoxide (DMSO) instead of water was utilised as a solvent. While undoubtedly an important result, DMSO is unquestionably less environmentally friendly than water. Moreover, the separation of HMF from DMSO is often a cost-intensive process.

In summary, despite the drop in HMF selectivity at very high glucose conversions, to the best of our knowledge, HMF yields as high as 45% (Figure 6) constitute the highest HMF yields reported so far for the glucose conversion performed in water with a standard batch reactor operating with a conventional heating system. Similar high yields of HMF produced from glucose in water were obtained in the presence of phosphate-niobia catalysts. However, the process requires high catalyst loadings (e.g. catalyst/substrate ratio = 10).[38] Yields similar to those

presented in this report were only attained with the use of organic solvents[7,18,19,22] or biphasic systems.[23,25,29] Notably, in the case of biphasic systems, the continuous removal of HMF from the sugar-containing aqueous phase greatly contributes to even higher HMF yields than those presented here. Nonetheless, this feature is rather associated with the reaction engineering than intrinsic catalyst performance

The co-operation of CA and anatase

To shed light on the individual roles of citric acid and anatase in the conversion of glucose to HMF in the presence of the hybrid-TiO_2, our strategy was to examine the system beginning with a mixture of i-TiO_2 and citric acid in water. Table 2 shows the glucose conversion and the selectivity to HMF and fructose.

Table 2. Selectivity to 5-hydroxymethylfurfural (HMF) and fructose at similar glucose conversions.

Entry	Catalytic system	X (%)	Selectivity (% mol C)	
			Fructose	HMF
1	Citric acid[b]	7	10	31
2	i-TiO_2[a]	22	26	5
3	i-TiO_2 + Citric acid[b]	23	18	41
4	Hybrid-TiO_2[a]	28	17	48

[a] Reaction temperature 130 °C. [b] Reaction temperature 140 °C. Temporal reaction monitoring profiles are presented in Supporting Information (Figure S3).

CA exhibits a modest catalytic activity for glucose conversion (Entry 1). In this experiment, a 7% conversion of glucose was achieved at 140 °C for 7 h, the selectivity to HMF was 31%. In the presence of i-TiO_2, a 22% conversion of glucose into fructose (at 26% selectivity) and HMF (at 5% selectivity) was obtained (Entry 2). The presence of citric acid in the catalytic system (Entry 3 and 4) significantly improved selectivity to HMF by eight- to nine-times, compared to i-TiO_2 (Entry 2). As revealed by FTIR spectroscopy, CA adsorbs on the surface i-TiO_2 creating surface citrate species comparable to those found in hybrid-TiO_2 (Figure S2). Nonetheless, hybrid-TiO_2 is more active and selective to HMF than the mixture of i-TiO_2 and CA. In fact, a 23% conversion was only achieved in the presence of i-TiO_2 and CA (Entry 3) at 140 °C for 3 h. In contrast, for hybrid-TiO_2 (Entry 4), a 28% conversion was achieved under milder conditions (130 °C for 30 min). Overall, these results indicate a co-operative effect of anatase surface, which appears to catalyse the isomerisation of glucose into fructose, and CA that catalyses the conversion of fructose into HMF. In this context, compared to i-TiO_2, the better performance of hybrid-TiO_2 for the isomerisation step seems to be associated with the presence of anatase Lewis acid sites. Importantly, the results from Table 2 starkly contrast to those by Souza and co-workers,[8] who showed highly concentrated aqueous organic acids solutions (e.g. a 20% acetic acid/water or 50% lactic acid/water) to be capable of catalysing the conversion of hexoses into HMF. In that report, HMF yields up to 43% and 26% from fructose and glucose, respectively, were reported.

Catalyst recycling experiments

The potential reusability of hybrid-TiO_2 was explored by four successive catalyst uses. After each catalyst test, hybrid-TiO_2 was collected, washed with water, and dried at 140 °C overnight. Logically, the spent catalyst was not calcined to remove humins, as a common practice in this research field, as this would also decompose the CA content chemically bounded to TiO_2. Figure 7 summarises the results obtained from the recycling experiments carried out in the presence of hybrid-TiO_2.

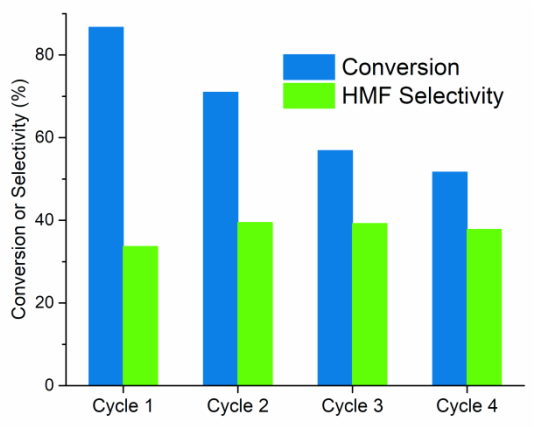

Figure 7. Catalyst recycling tests over hybrid-TiO_2. Reaction conditions: water (160 mL), glucose (3.3 g), hybrid-TiO_2 (3.0 g), 500 rpm, 140 °C for 5 h.

Figure 7 shows a gradual decrease in glucose conversion while HMF selectivity remains approximately constant after each recycling run. Surprisingly, even for Cycle 4, selectivity to HMF (38%) are much superior to those achieved by i-TiO_2 in the first use at similar glucose conversion (selectivity to HMF: 16%, as inferred from Figure 6f, results for the reaction mixture at 3h). As demonstrated by the XRD patterns and HR-TEM imaging, hybrid-TiO_2 retained its structural features throughout the recycling experiments (Figures S4 and S5). Nonetheless, a change in the material colour was observed. The material transformed from white (fresh catalyst) to pale yellow and finally brown in colour after the 4th recycling run. Both colour change and a decline in conversion can be attributed to the accumulation of humins over the catalysts surface, which blocks the catalysts active sites.[1,4,40,42,43] However, even without calcination steps to remove humins,[43] hybrid-TiO_2 could still enable an HMF yield of 20% after the 4th reaction run.

The fate of CA throughout the recycling experiment

CA is a strong chelating agent which has found use as a stabiliser in several nanomaterial syntheses. This fact cast doubts on the possibility of leaching of CA from the hybrid-TiO_2. In fact, Mudunkotuwa and Grassian[44] found the adsorption of citric acid to be an irreversible process at room temperature, regardless of the medium pH. However, despite these previous results, the fact that a suprastoichiometric quantity of CA was employed in the synthesis of hybrid-TiO_2 suggests that leaching of CA from the catalyst may eventually take place in the catalyst recycling. To address whether there is CA leaching from hybrid-TiO_2, the material was subjected to a hydrothermal treatment with no added

glucose simulating the catalyst test conditions (500 rpm, 140 °C, 7 h). We chose this approach to avoid deposition of humins on the material, which complicates the evaluation of CA leaching by TGA-MS or elemental analysis. Following the simulated reaction tests, the fresh and spent catalysts were characterised by elemental analysis (Table 3) and thermogravimetric analysis (TGA-MS, Figure 8).

Table 3. C-content present in hybrid-TiO_2 before and after simulated reaction tests.

Entry	Material	C-content (%)
1	Fresh hybrid-TiO_2	4.5 ± 0.1
2	After 1st simulated reaction	3.1 ± 0.1
3	After 2nd simulated reaction	2.5 ± 0.1
4	After 3rd simulated reaction	2.1 ± 0.1

[a] Simulated reaction conditions: hybrid-TiO_2 (3.0 g), H_2O (160 mL), 140 °C, 500 rpm, 7 h.

Table 3 reveals that C-content present in the hybrid-TiO_2 markedly decreased (from 4.5 ± 0.1% to 3.1 ± 0.1%) after the first simulated reaction run. Importantly, in the successive runs, the C-content reduced more gradually (from 3.1 ± 0.1% to 2.5 ± 0.1% for the 2nd run, and to 2.1 ± 0.1% for the 3rd run). Despite the decrease in C-content in hybrid-TiO_2 no substantial change in the FTIR spectrum of the spent catalyst was detected (Figure S2).
Figure 8 shows the TGA profiles for the materials. According to the MS results, the first weight loss (30-120 °C) is associated with the elimination of water. The second and third weight losses, (170-500 °C) are related to the thermal decomposition of CA, as inferred from the MS results for the CO_2 monitoring. Interestingly, the onset temperature in which the CO_2 release initiates gradually shifts (from ca. 170 to 200 °C) upon the catalyst reutilisation (as indicated by a blue-coloured arrow in Figure 8c). This observation indicates that the remaining CA in the hybrid-TiO_2 is slightly more strongly bounded to anatase structure and, therefore, still playing a role in the structural stabilisation of hybrid-TiO_2 under reaction conditions. Moreover, XRD analysis of spent hybrid-TiO_2 reveals that the apparent crystallite size underwent no significant change throughout the recycling experiments (5 nm, Table S2). As expected, the decrease in the second and third weight losses agrees with the reduction in C-content observed for the hybrid-TiO_2 material after the simulated reactions. Nonetheless, there is a mismatch between the profile of C-content decrease and the sustainability of the catalyst performance (Figure 8). This observation suggests that the loss in catalytic performance should be associated not only with the leaching of loosely-bound CA but also with other transformations in the anatase structure, which are difficult to resolve using XRD owing to the nanocrystalline nature of hybrid-TiO_2.

To shed light on the changes occurring in the local order of Ti(IV) in the materials upon the leaching of loosely-bounded CA, XANES analyses of the spent catalysts obtained from the simulated reactions were performed. The pre-edge features of the normalised Ti-edge XANES spectra are presented in Figure 9.

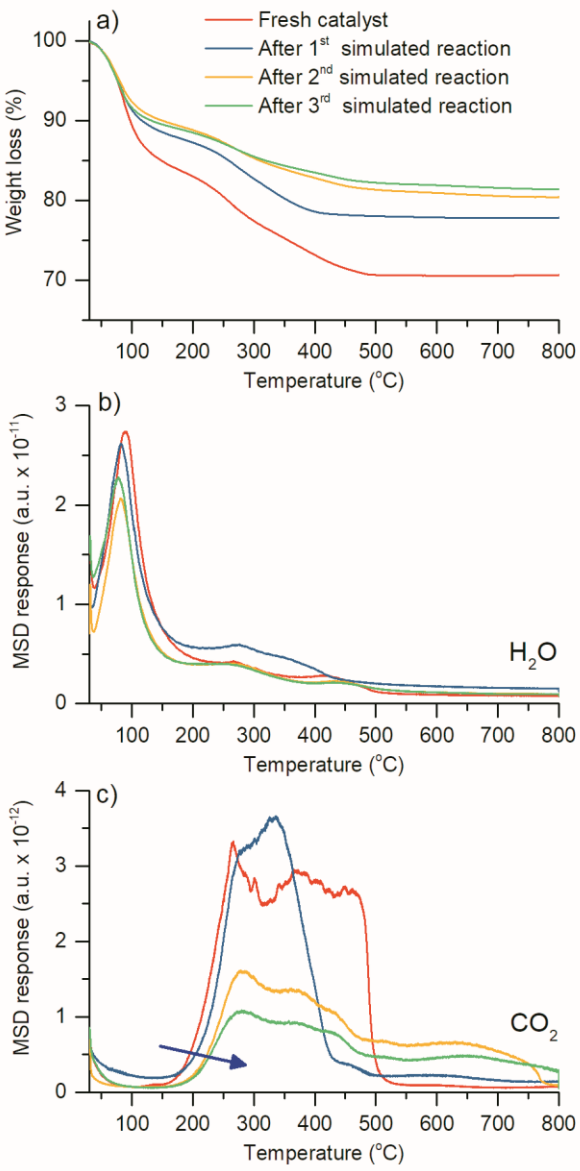

Figure 8. TGA-MS of hybrid-TiO_2 before and after simulated reactions: a) TGA curves; b) MSD response for water (m/z: 18); c) MSD response for CO_2 (m/z: 44). The blue-colour arrow on the diagram 'c' indicates the shift of onset temperature for the CA decomposition. Simulated reaction conditions: H_2O (160 mL), hybrid-TiO_2 (3.0 g), 500 rpm, 140 °C, 7 h.

Throughout the recycling experiments, the pre-edge features of the hybrid-TiO_2 tend to near to those of i-TiO_2, indicating that there is a slight decrease in the quantity of fivefold coordinated Ti(IV) centres. This observation suggests that the strong interaction between Ti(IV) centres and citric acid is conducive to the preservation of the nanostructured features of hybrid-TiO_2 throughout the recycling experiments. Moreover, the resilience of fivefold coordinated Ti(IV) centres after successive cycles of hydrothermal treatment (simulated reactions) demonstrates the stability of these water-tolerant Lewis sites.

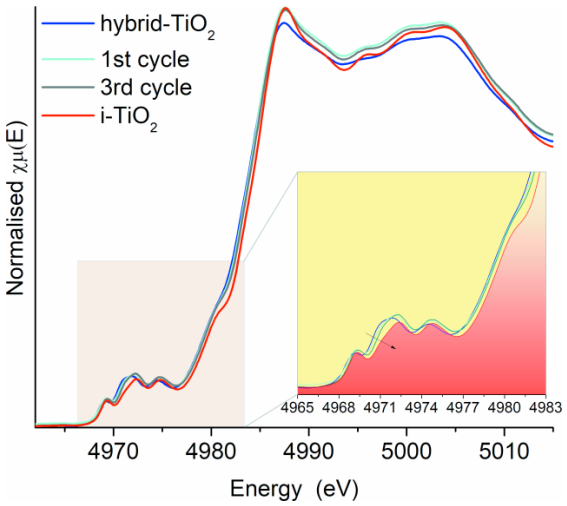

Figure 9. Pre-edge features of Ti K-edge XANES spectra of the as-synthesised hybrid-TiO_2 catalysts (dark blue), after 1 cycle of simulated catalytic reaction (light blue), after the third cycle (grey) and i-TiO_2 (red, provided for comparison).

Conclusions

The synthesis of anatase in the presence of a suprastoichiometric quantity of CA generates a nanocrystalline hybrid-organic-inorganic material with improved catalytic properties for the conversion of glucose into HMF in water under mild conditions. In fact, hybrid-TiO_2 enabled high HMF yields (45%) in a monophasic batch reactor. Surprisingly, even after four cycles of catalyst use, without a calcination step to remove humins from the catalyst surface, hybrid-TiO_2 was still able to render a 29% HMF yield.

Ti-edge XANES was a powerful tool for the characterisation of Ti coordination showing an enhanced presence of five-fold coordinated Ti(IV) centres that are associated with the formation of Lewis acid sites on the anatase surface of the hybrid-TiO_2. The current results provide compelling evidence for the stability of water-tolerant Lewis acidity of hybrid-TiO_2.

Besides the key roles of CA in the formation of Lewis sites, CA also retards the degradation of the catalysts structural features throughout the recycling experiments. In addition, as the hybrid-TiO_2 is not calcined, but employed in the reaction as synthesised, we could verify the hypothesis that Brønsted acid sites associated with the presence of CA in the hybrid-TiO_2 play a role in the conversion of fructose into HMF. Nonetheless, more work is still required for a clear designation of the level of participation of leached and TiO_2-bounded CA species in the catalysis for the conversion of fructose into HMF.

Experimental Section

Catalysts Synthesis

TiO_2 catalysts were synthesised via sol-gel (i-TiO_2) and hydrothermal methods (hybrid-TiO_2). Both procedures are described hereafter. All chemicals purchased were used without further purification.

For the synthesis of hybrid-TiO_2, $TiCl_4$ (9 mL, 82 mmol, Merck) was poured into ice-cold deionised water (200 mL) under vigorous stirring. Next, citric acid (17.3 g, 90 mmol, Sigma-Aldrich) was immediately added to the mixture. In sequence, the suspension was refluxed at 140 °C for 16 h. Finally, the solid was washed with hot water several times until pH 7. The solid was dried in an oven at 140 °C overnight, rendering the hybrid-TiO_2, which was employed here as the catalyst.

For the synthesis of i-TiO_2, titanium isopropoxide (12 mL, Aldrich) was added to 2-propanol (12 mL, Merck) under stirring. Water (6 mL) was added to the mixture. Stirring was maintained for 1 h. The solution was then allowed to age for 24 h. The product was then dried at 80 °C for 6 h and calcined at 450 °C for 16 h.

Catalyst Characterisation

X-ray diffraction (XRD) patterns were obtained at the XPD beamline at the LNLS/CNPEM. The beamline energy was 8.0 keV and the XRD data collected using a linear detector (Mythen 1k). Identification of crystalline phases was obtained from ICSD files. The crystallite sizes for TiO_2 were estimated by using the Scherrer equation.

Nitrogen adsorption-desorption isotherms were measured at -196 °C on a Quantachrome Autosorb-1C automatic analyser. Samples were degassed at 120 °C for 13 h before isotherms were measured. The specific surface area values were determined using the BET model. The total pore volume was derived from the amount of gas absorbed at a relative pressure of $P/P_0 = 0.95$.

The morphology of the TiO_2 crystallites was investigated by using an HR-TEM JEOL-JEM 2100F operating at 200 kV at the LNNano/CNPEM, with a resolution of 0.19 nm.

XAFS experiments were carried out at the Brazilian synchrotron laboratory (LNLS) at the XAFS1 beamline. The measurements at the Ti K-edge (4966 eV) were carried out in transmission mode at ambient temperature. The monochromator energy calibration was verified measuring a Ti metal foil. Samples were prepared by deposition of powders onto a micropore membrane. The spectra were analysed using Athena and Artemis software packages version 0.9.25.

FTIR spectra were collected on a Nicolet FT-IR-6700 spectrometer in the range of 4000 to 1000 cm^{-1} with a resolution of 2 cm^{-1}. and 128 scans for signal accumulation. Sample preparation: sample powder was pressed, rendering a thin pellet. The sample pellet was transferred into a homemade IR cell equipped with NaCl windows. First, the sample was evacuated at 120 °C for 22 h under dynamic vacuum (2.10^{-5} mbar). After cooling to room temperature, the sample spectrum was obtained. Then, the samples were exposed to pyridine vapor until the equilibrium vapor pressure and the cell was kept under this condition for an additional 24 h. Next, the IR cell was heated up to 120 °C for 22 h under dynamic vacuum (2.10^{-5} mbar). After cooling down to room temperature, the IR spectrum of adsorbed pyridine on the sample was collected.

Thermogravimetric analyses were carried out on a NETZSCH TG 209F1 Libra coupled to an MS detector. TG curves were obtained from the samples (40 mg) heated at 10 °C min^{-1} from 30 to 800 °C under synthetic air flow in a ceramic sample holder.

CHN/O elemental analyses were performed in triplicate for samples (2 mg) on a Vario Micro Cube elemental analyser (Elementar). Average values of the triplicate measurements are reported.

Catalyst Tests

The catalytic tests were performed using a Hastelloy batch reactor (300 mL, Parr Instruments). Glucose (Sigma) and catalyst were loaded into the reactor with an appropriated catalyst/glucose mass ratio, with 160 mL of total reaction volume (2 wt% glucose concentration). The reactor was purged with nitrogen and the temperature raised to reaction

temperature (120, 130 or 140 ^{0}C) with an agitation speed of 500 rpm. At each point of the kinetic curve, a sample from the reactor was taken for product and glucose quantification. Therefore, each kinetic curve was done by repeating several times an experiment under a given condition for various durations.

HPLC analyses were performed using a Waters 1525 chromatograph at the CTBE/CNPEM equipped with Aminex HPX-87H – Bio-rad capillary column and Acclaim 120 C18 Dionex column for analysis using refractive index (RI) and UV detectors. Glucose conversion (X,% mol/mol), product yield (Y,%mol/mol) and selectivity (S,%mol/mol) were determined according to the equations:

$$X = \left(1 - \frac{G_f}{G_0}\right) \times 100$$

$$Y_i = \frac{\#C_i}{6}\frac{P_i}{G_0} \times 100$$

$$S_i = \frac{Y_i}{X} \times 100$$

where G_0 (mol/L) denotes the glucose concentration in the feed and G_f (mol/L) denoting after reaction values. *#Ci* and *Pi* are the carbon number and the concentration of the product *i* (mol/L) (fructose, HMF, levulinic acid, etc.), respectively. The standard deviation was calculated, and the maximum values are given as follows: ± 3% for glucose conversion, ±1% for HMF yield and finally, ±0.8% for fructose yield.

Acknowledgements

The authors are grateful to LNLS/CNPEM and CNPq for the financial support, CTBE/CNPEM for chromatographic analysis of reaction products and LNNano for the TEM microscope. We would also like to thank Guilherme. P. Nogueira for the catalyst preparation and reactions. RR acknowledges the support provided by the ERC Consolidator Grant (LIGNINFIRST, Project Number: 725762) for this collaborative work.

Keywords: anatase, water-resistant Lewis acid, hydrothermal synthesis, citric acid, glucose dehydration, HMF

[1] A. A. Rosatella, S. P. Simeonov, R. F. M. Frade, C. A. M. Afonso, *Green Chem.* **2011**, *13*, 754-793.

[2] I. Jiménez-Morales, J. Santamaría-González, A. Jiménez-López, P. Maireles-Torres, *Fuel* **2014**, *118*, 265–271.

[3] M. J. Climent, A. Corma, S. Iborra, *Chem. Rev.* **2011**, *111*, 1072–133.

[4] R. Van Putten, J. C. Van Der Waal, E. De Jong, C. B. Rasrendra, H. J. Heeres, J. G. De Vries, Chem. Rev., 2013, 113, 1499–1597.

[5] M. Watanabe, Y. Aizawa, T. Iida, R. Nishimura, H. Inomata, *Appl. Catal. A Gen.* **2005**, *295*, 150–156.

[6] R. Noma, K. Nakajima, K. Kamata, M. Kitano, S. Hayashi, M. Hara, *J. Phys. Chem. C* **2015**, 117, 16028–16033.

[7] S. Dutta, S. De, A. K. Patra, M. Sasidharan, A. Bhaumik, B. Saha, *Appl. Catal. A Gen.* **2011**, *409–410*, 133–139.

[8] R. L. de Souza, H. Yu, F. Rataboul, N. Essayem, *Challenges* **2012**, *3*, 212–232.

[9] A. Chareonlimkun, V. Champreda, A. Shotipruk, N. Laosiripojana, *Bioresour. Technol.* **2010**, *101*, 4179–86.

[10] G. Yang, E. A. Pidko, E. J. M. Hensen, *ChemSusChem* **2013**, *6*, 1688–1696.

[11] E. A. Pidko, V. Degirmenci, E. J. M. Hensen, *ChemCatChem* **2012**, *4*, 1263–1271.

[12] G. Yang, E. A. Pidko, E. J. M. Hensen, *J. Catal.* **2012**, *295*, 122–132.

[13] X. Qi, M. Watanabe, T. M. Aida, R. L. Smith, *Catal. Commun.* **2008**, *9*, 2244–2249.

[14] E. F. L. J. Anet, in *Adv. Carbohydr. Chem.*, **1964**, pp. 181–218.

[15] C.-H. Kuo, A. S. Poyraz, L. Jin, Y. Meng, L. Pahalagedara, S.-Y. Chen, D. A. Kriz, C. Guild, A. Gudz, S. L. Suib, *Green Chem.* **2014**, *16*, 785.

[16] Y. Yang, C. Hu, M. M. Abu-Omar, *J. Mol. Catal. A Chem.* **2013**, *376*, 98–102.

[17] a) Y. J. Pagán-Torres, T. Wang, J. M. R. Gallo, B. H. Shanks, J. A. Dumesic, *ACS Catal.* **2012**, *2*, 930–934; b) R. Carrasquillo-Flores, M. Käldström, F. Schüth, J. A. Dumesic, R. Rinaldi, *ACS Catal.* **2013**, *3*, 993-997.

[18] L. Hu, G. Zhao, X. Tang, Z. Wu, J. Xu, L. Lin, S. Liu, *Bioresour. Technol.* **2013**, *148*, 501–507.

[19] M. Zhang, K. Su, H. Song, Z. Li, B. Cheng, *Catal. Commun.* **2015**, *69*, 76–80.

[20] T. Wang, Y. J. Pagán-Torres, E. J. Combs, J. A. Dumesic, B. H. Shanks, *Top. Catal.* **2012**, *55*, 657–662.

[21] L. Qi, Y. F. Mui, S. W. Lo, M. Y. Lui, G. R. Akien, I. T. Horváth, *ACS Catal.* **2014**, 1470–1477.

[22] J. Liu, H. Li, Y.-C. Liu, Y.-M. Lu, J. He, X.-F. Liu, Z.-B. Wu, S. Yang, *Catal. Commun.* **2015**, *62*, 19–23.

[23] L. Atanda, A. Silahua, S. Mukundan, A. Shrotri, G. Torres-Torres, J. Beltramini, *RSC Adv.* **2015**, *5*, 80346–80352.

[24] J. Zhang, L. Lin, S. Liu, *Energy Fuels* **2012**, *26*, 4560–4567.

[25] L. Atanda, S. Mukundan, A. Shrotri, Q. Ma, J. Beltramini, *ChemCatChem* **2015**, *7*, 781–790.

[26] K. Nakajima, R. Noma, M. Kitano, M. Hara, *J. Phys. Chem. C* **2013**, *117*, 16028–16033.

[27] Luis Augusto Barbosa Cortez, *Catalytic Dehydration of C6 Carbohydrates for the Production of Hydroxymethylfurfural (HMF) as a Versatile Platform Chemical*, PhD Thesis, São Paulo, **2010**.

[28] E. Nikolla, Y. Román-Leshkov, M. Moliner, M. E. Davis, *ACS Catal.* **2011**, *1*, 408–410.

[29] K. Nakajima, R. Noma, M. Kitano, M. Hara, *J. Mol. Catal. A Chem.* **2014**, *388–389*, 100–105.

[30] H. Shintaku, K. Nakajima, M. Kitano, N. Ichikuni, M. Hara, *ACS Catal.* **2014**, *4*, 1198–1204.

[31] Y. Li, N. H. Lee, D. S. Hwang, J. S. Song, E. G. Lee, S. J. Kim, *Langmuir* **2004**, *20*, 10838–10844.

[32] H. Yin, Y. Wada, T. Kitamura, T. Sumida, Y. Hasegawa, S. Yanagida, *J. Mater. Chem.* **2001**, *12*, 378–383.

[33] Y. Liu, C. yan Liu, Z. ying Zhang, *Chem. Eng. J.* **2008**, *138*, 596–601.

[34] F. Leroux, P. J. Dewar, M. Intissar, G. Ouvrard, L. F. Nazar, *J. Mater. Chem.* **2002**, *12*, 3245–3253.

[35] Z. Y. Wu, G. Ouvrard, P. Gressier, C. R. Natoli, *Phys. Rev. B* **1997**, *55*, 10382–10391.

[36] F. Farges, G. E. Brown, J. J. Rehr, *Phys. Rev. B* **1997**, 56, 4,1809-1819.

[37] M. Kitano, K. Nakajima, J. N. Kondo, S. Hayashi, M. Hara, *J. Am. Chem. Soc.* **2010**, *132*, 6622–6623.

[38] K. Nakajima, Y. Baba, R. Noma, M. Kitano, J. Kondo, S. Hayashi, M. Hara, *J. Am. Chem. Soc.* **2011**, *133*, 4224–4227.

[39] L. Atanda, A. Shrotri, S. Mukundan, Q. Ma, M. Konarova, J. Beltramini, *ChemSusChem* **2015**, *8*, 2907–2916.

[40] T. Wang, M. W. Nolte, B. H. Shanks, *Green Chem.* **2014**, *16*, 548–572.

[41] S. Dutta, S. De, A. K. Patra, M. Sasidharan, A. Bhaumik, B. Saha, *Appl. Catal. A Gen.* **2011**, *409–410*, 133–139.

[42] A. Mukherjee, M.-J. Dumont, V. Raghavan, *Biomass and Bioenergy* **2014**, *72*, 143–183.

[43] C.-H. Kuo, A. S. Poyraz, L. Jin, Y. Meng, L. Pahalagedara, S.-Y. Chen, D. A. Kriz, C. Guild, A. Gudz, S. L. Suib, *Green Chem.* **2014**, *16*, 785.

[44] I. A. Mudunkotuwa, V. H. Grassian, *J. Am. Chem. Soc.* **2010**, *132*, 14986–14994.

[45] F. Zaera, *Chem. Soc. Rev.* **2014**, *43*, 7624-7663.

Entry for the Table of Contents
Layout 1:

FULL PAPER

With a lemon please! Herein, citric acid was employed in a facile hydrothermal synthesis method for the production of a hybrid-organic-inorganic anatase. This material was directly studied here as the catalyst for the conversion of glucose to HMF. Yields up to 45% at glucose conversions up to 75% were achieved in water at 130 °C in a monophasic batch reactor.

Carlos A. S. Lanziano, Silvia F. Moya, Dean H. Barrett, Erico Teixeira-Neto, Reginaldo Guirardello, Felipe de Souto da Silva, Roberto Rinaldi and Cristiane B. Rodella**

Page No. – Page No.

Hybrid-organic-inorganic anatase as a bifunctional catalyst for enhanced production of HMF from glucose in water